Seismolab

On the conditions for pore fluid stabilisation of shear failure in crustal rock

Franciscus M. Aben & Nicolas Brantut

Contact: f.aben@ucl.ac.uk

We study the coupling of localised brittle deformation (i.e., faulting) and pore fluids by the process known as **dilatancy strengthening**. Dilatancy encompasses small-scale brittle deformation near the rupture tip that increases the pore volume in a fault zone. The additional pore volume acts as a sink for pore pressure when the fault zone is partially or entirely undrained. A drop in pore pressure locally increases the fault normal stress, increasing the shear resistance. This **potentially stabilises and inhibits the failure process**. Dilatancy stabilisation is a transient process, as the extraneous shear resistance vanishes when pore pressure recovers to its initial value. Hence, it provides a mechanism for an extended earthquake precursor time.
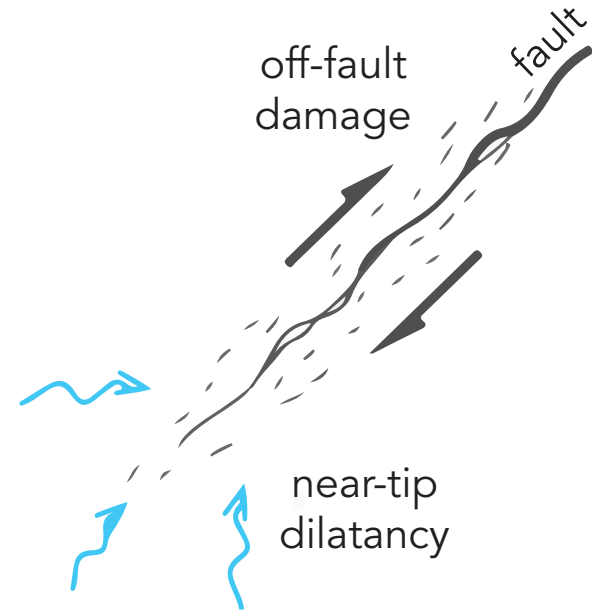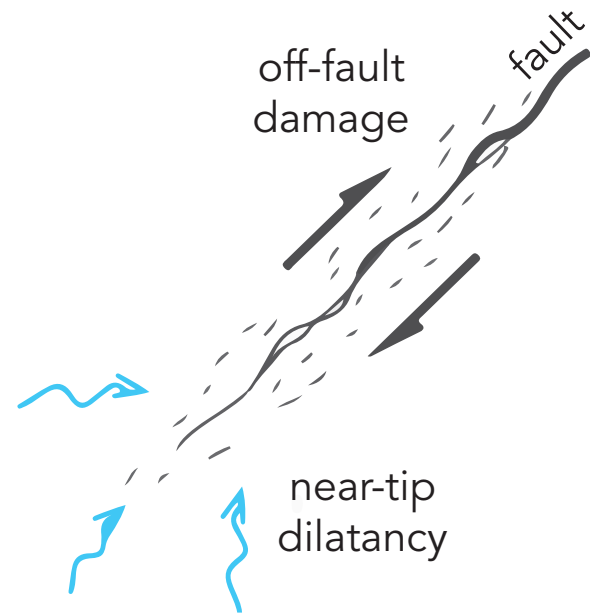

off-fault damage

fault

near-tip dilatancy

Sketch showing near-tip damage in a fault that acts as a pore pressure sink

UCL

A better understanding of pore fluid stabilisation during shear failure **requires quantification of the transient pore pressure change** in the fault zone.

Here, we present novel laboratory measurements of the on-fault pore pressure during stabilised and dynamic shear failure under triaxial conditions. These measurements show the evolution of effective fault normal stress during stabilised and dynamic failure.

We use this data to calibrate a spring-slider model that allows for dilatancy. This model **may then be used to provide experimental-based predictions of precursor times**.
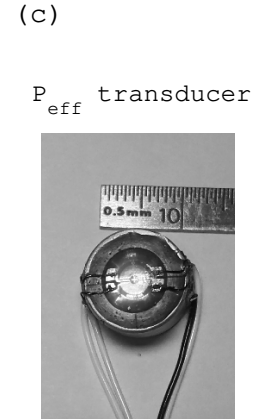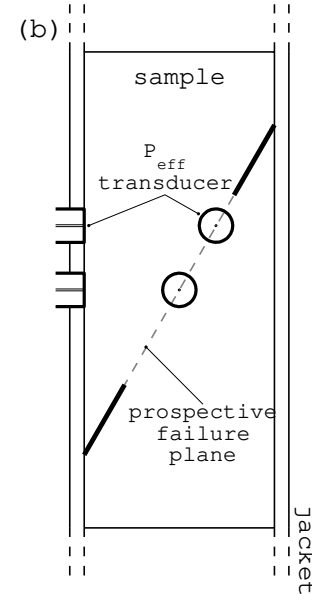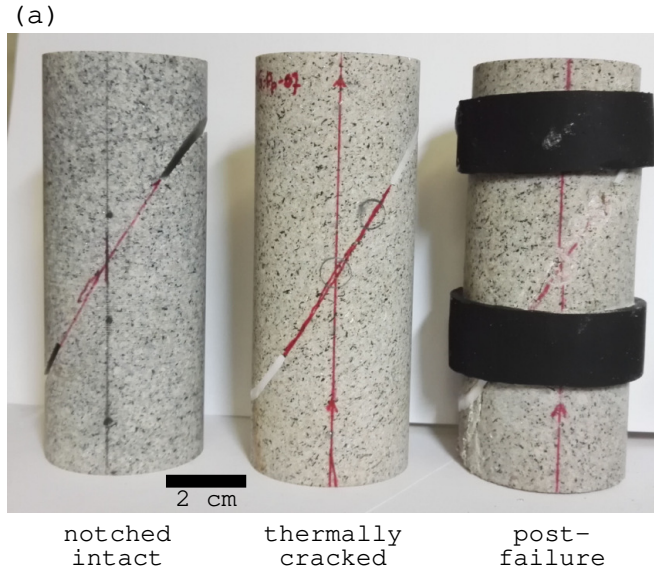

off-fault damage

fault

near-tip dilatancy

Sketch showing near-tip damage in a fault that acts as a pore pressure sink
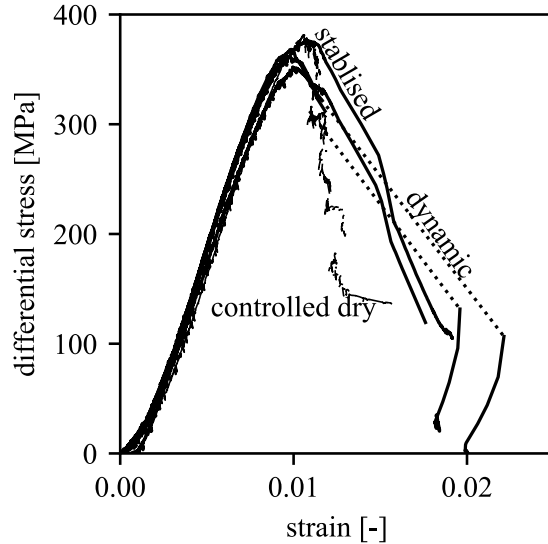
UCL

We measure the on- and off-fault pore pressure during a series of shear failure experiments on thermally cracked water saturated Westerly granite in a conventional triaxial loading apparatus. We test different combinations of confining pressure P_c and imposed pore pressure, while keeping the effective pressure constant to $P_{eff} = 40$. We imposed a displacement rate of 1×10^{-6} mm s^{-1}. An AE-controlled shear failure test on a dry sample at $P_c = 40$ MPa provides a reference. Pore pressure was measured using novel in-house produced P_{eff} sensors (see Brantut 2020).

(a): Notched Westerly granite samples that are intact (left), thermally cracked (center) and thermally cracked and failed under triaxial loading conditions (right).

(b): Schematic of the sample setup, with two effective pressure transducers on the prospective failure plane, and two transducers on the hanging block of the sample.

(c): Photo of an effective pressure transducer.

(a)

2 cm

notched
intact

thermally
cracked

post-
failure

(b)

sample

P_{eff}
transducer

prospective
failure
plane

jacket

(c)

P_{eff} transducer

Stress-strain data of five failure experiments at P_{eff} = 40 MPa: One controlled dry failure following the approach of Lockner et al. (1991), two stabilised failures (P_c = 100 and 120 MPa), and two dynamic failures (P_c = 60 and 70 MPa).

We observe stabilised and dynamic failure at P_{eff} = 40 MPa, with stabilised failure occurring at higher P_c.

The pore volume increase measured after failure does not correlate to stabilised or dynamic failure.
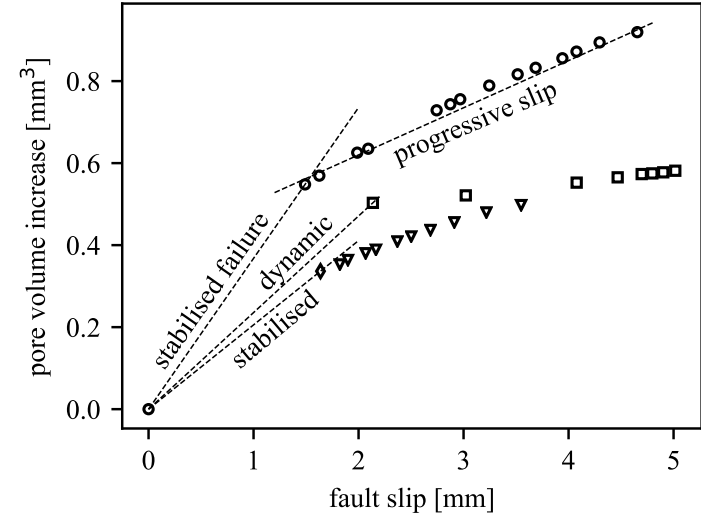
Pore volume increase as a function of fault slip for two stabilised failures and one dynamic failure. Pore volume was measured during progressive slip after failure. Dashed lines give a first order estimate of porosity increase with slip during failure and progressive slip. We ascribe variations between samples to varying fault zone roughness.

Axial displacement was arrested and pore pressure was allowed to equilibrate in order to measure the pore volume increase.

- During stabilised failures, the fault zone pore pressure decrease provides a shear resistance that is sufficiently high to stabilise the fault. Maximum pore pressure decrease is around 40 MPa.

- During dynamic failure, the pore pressure in the fault zone reaches 0 MPa so that the dilatancy-induced shear resistance vanishes and the fault becomes unstable.

For dynamic failures, the potential pore pressure drop was thus larger than the initial pore pressure.

stabilised failure — dynamic failure
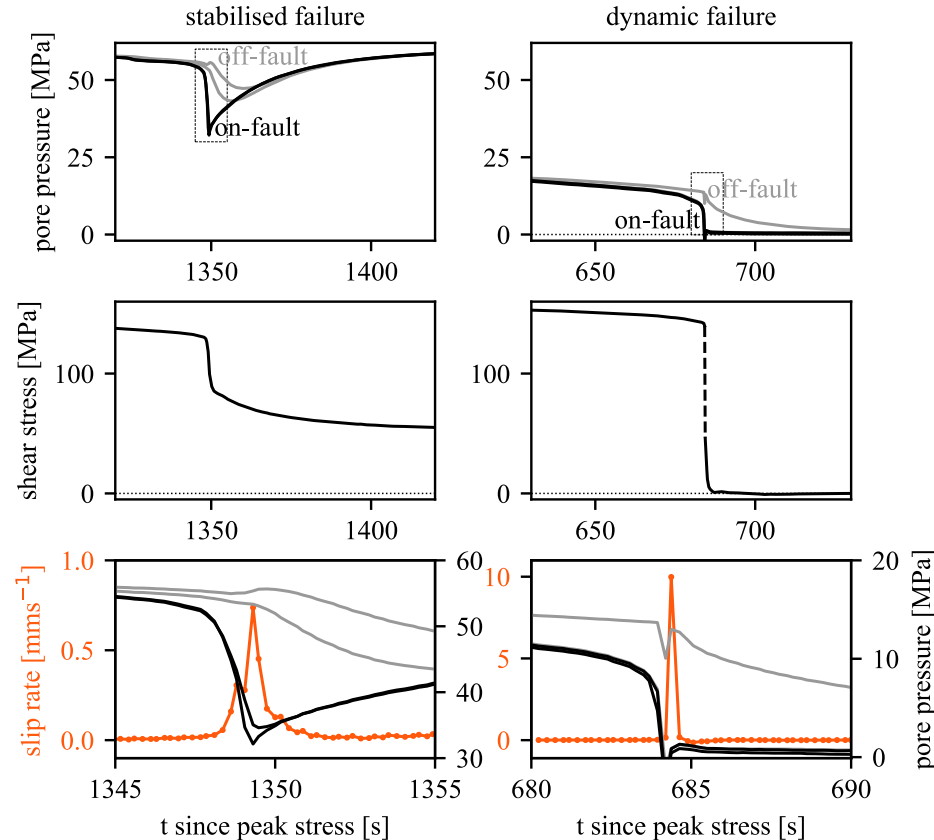
Pore pressure, shear stress, and slip rate records for a stabilised failure at P_c = 100 MPa (left) and a dynamic failure at P_c = 60 MPa (right). On-fault pressure transducers (black curves) record a steeper and larger drop in pore pressure relative to off-fault pressure transducers (gray curves). The bottom panel is a magnification indicated in the top panel.

The absence on the fault of an immediate pore pressure recovery after dynamic failure indicates local vaporisation of pore fluids (Brantut 2020).
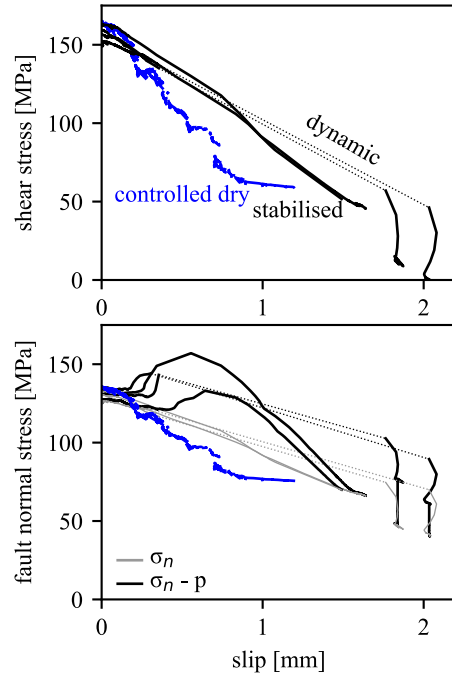
Shear stress (top) and fault normal stress (bottom) versus fault slip. The effective normal stress (black curves) is the difference in fault normal stress (gray curves) minus the on-fault pore pressure.

The recorded on-fault pore pressure allows us to track the effective fault normal stress during failure (left).
We ascribe the drop in shear stress during controlled dry failure to the loss of cohesion. For stabilised failure, the decrease in shear stress is some combination of the loss of cohesion and an extraneous shear resistance from the transient increase in frictional strength. This is best understood in a classic Mohr diagram (below), where we observe that a section of the post-failure stress path traverses along the frictional strength envelope.
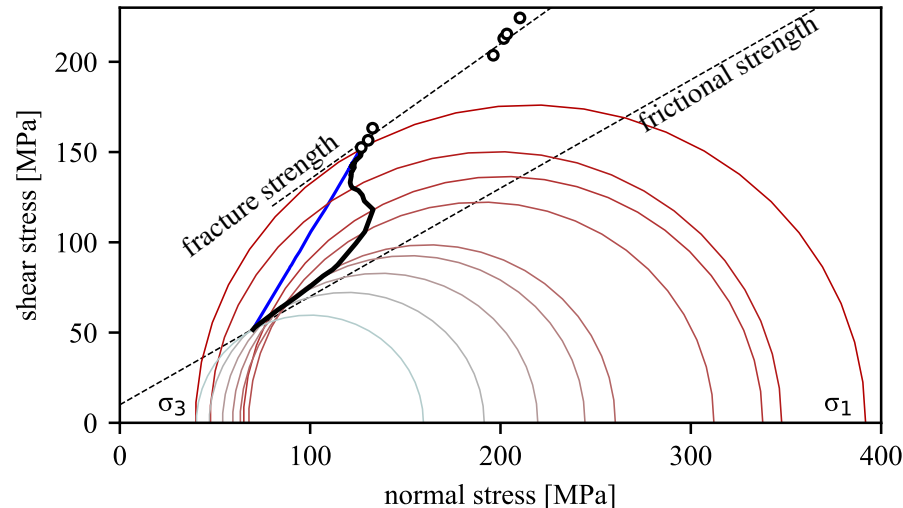
Failure stress path for an experimental dry failure (blue curve) and a stabilised failure (black curve). Mohr circles in red are shown along the stabilised failure path. Fracture strength (open circles) from this work, frictional strength from Byerlee (1967).

We now study a simple 1D spring-slider model to illustrate the additional shear resistance resulting from the transient increase in frictional strength caused by dilatancy:

$y = 0, p = p_0$

fluid inlet

intact rock

S, κ

spring stiffness (driving force)   slip-dependent cohesion   pore pressure dependent friction   damping term

$$k(v_\infty t - \delta) \quad - \quad \tau_{\mathrm{p}} \quad - \quad \mu(\sigma_{\mathrm{n}} - p) \quad - \quad \eta v = 0$$

k

$y = L$

w $S_{\mathrm{f}}, \mu, \tau_{\mathrm{p}}$ fault zone

k ...... stiffness
v_∞ ..... driving velocity
t .... time
δ ...... fault slip
τ_{p} ...... cohesion shear stress drop
μ ...... coeff. of residual friction
σ_{n} ...... fault normal stress
p ...... pore pressure
η ...... viscosity
v ...... slip velocity
κ ...... permeability
S ...... storage capacity
y ...... fault normal distance
w ......fault zone width

Outside the fault zone, the pore pressure is governed by a diffusion equation:

$$\frac{\partial p}{\partial t} = \frac{\kappa}{\eta S} \frac{\partial^2 p}{\partial y^2}$$

Inside the fault zone, the pore pressure is given by:

$$\frac{\partial p}{\partial t} = -\frac{v}{S_{\mathrm{f}}} \frac{d\phi}{d\delta} - \frac{2\kappa}{w\eta S_{\mathrm{f}}} \frac{\partial p}{\partial y}$$

UCL
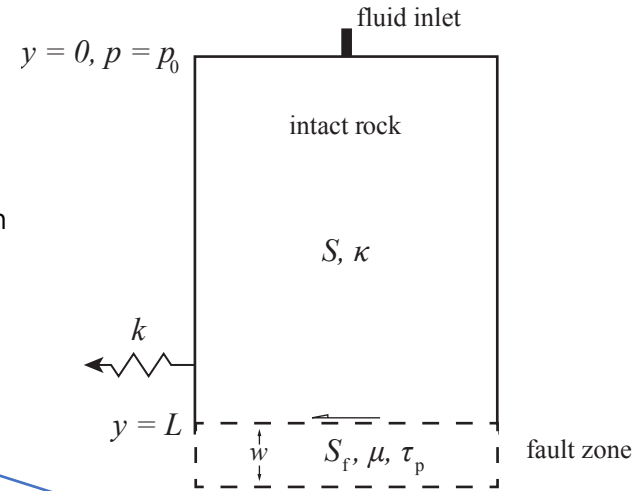
Thanks to our on-fault pore pressure sensors, most variables in the spring-slider model have been recorded and have been presented here, except for the intact hydraulic properties (measured by Brantut 2020). The remaining unknown variables are the fault zone width w and fault zone storage capacity S_f. For now, we assume w = 3 mm.

We match the observed minimum on-fault pore fluid pressure and maximum fault slip velocity with those predicted by spring-slider simulations for a range of fault zone storage capacities. **This provides a surprisingly high estimate for the fault zone storage capacity between 0.15 x 10⁻⁹ Pa⁻¹ and 0.6 x 10⁻⁹ Pa⁻¹.**
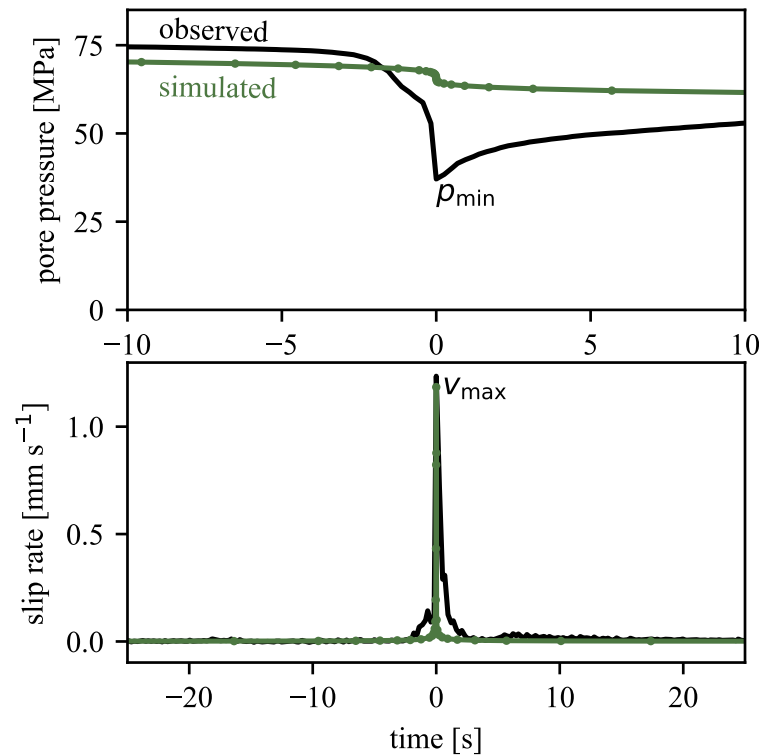
Observed and simulated pore pressure (top) and slip rate (bottom) during stabilised shear failure.

The maximum simulated slip rate matches best with the observed one with a fault zone storage capacity of around 0.56 x 10⁻⁹ Pa⁻¹, as shown here.
The minimum pore pressure matches best with a lower fault zone storage capacity of around 0.15 x 10⁻⁹ Pa⁻¹.

Misfits between the simulations and experimental data arise primarily from the assumption of a 1D model, simplification of the cohesion stress drop and slip-dependent porosity increase, and an assumed fault zone width.

Result summary

- Both dynamic and stabilised shear failure was observed in rupture experiments at P_{eff} = 40 MPa
- We have measured on-fault pore pressure changes up to 40 MPa during shear failure.
- We see that pore pressure drops to zero during dynamic failure, whereas it remains finite for stabilised failure.

Conclusion

- The transition from stable to dynamic failure in rupture experiments at P_{eff} = 40 Mpa occurs when the potential pore pressure drop is larger than the initial pore pressure, eliminating the effect of dilatancy stabilisation.
- 1D spring-slider simulations of our experiments suggest a fault zone storage capacity between 0.15 x 10^{-9} Pa^{-1} and 0.6 x 10^{-9} Pa^{-1}.
- Our experimental constraints on intrinsic fault zone properties during shear failure may be used to obtain earthquake precursor times (work in progress).

References

- Brantut 2020. Dilatancy-induced fluid pressure drop during dynamic rupture: Direct experimental evidence and consequences for earthquake dynamics, EPSL
- Lockner et al., 1991. Quasi-static fault growth and shear fracture energy in granite, Nature